Title

Free-breathing, motion-corrected, highly efficient whole heart T2 mapping at 3T with hybrid radial-cartesian trajectory.

Journal

Magnetic resonance in medicine, 75(1)

ISSN

0740-3194

Authors

Yang, Hsin-Jung
Sharif, Behzad
Pang, Jianing
et al.

Publication Date

2016

DOI

10.1002/mrm.25576

Peer reviewed

HHS Public Access

Author manuscript

Magn Reson Med. Author manuscript; available in PMC 2017 January 01.

Published in final edited form as:

Magn Reson Med. 2016 January ; 75(1): 126–136. doi:10.1002/mrm.25576.

Free-Breathing, Motion-Corrected, Highly Efficient Whole-Heart T_2 Mapping at 3T with Hybrid Radial-Cartesian Trajectory

Hsin-Jung Yang[*,†], **Behzad Sharif**[*,¶], **Jianing Pang**[*,¶], **Avinash Kali**[*,†], **Xiaoming Bi**[^], **Ivan Cokic**[*], **Debiao Li**[*,†,#], and **Rohan Dharmakumar**[*,#,**]

[*]Biomedical Imaging Research Institute, Dept of Biomedical Sciences, Cedars-Sinai Medical Center, Los Angeles CA 90048 USA

[†]Dept of Bioengineering, University of California, Los Angeles CA 90095 USA

[#]Dept of Medicine, University of California, Los Angeles CA 90095 USA

[^]MR R&D, Siemens Healthcare, Los Angeles, CA, USA

[**]Cedars-Sinai Heart Institute, Cedars-Sinai Medical Center, Los Angeles CA 90048 USA

Abstract

Purpose—To develop and test a time-efficient, free-breathing, whole-heart T_2 mapping technique at 3.0T.

Methods—ECG-triggered three-dimensional images were acquired with different T_2 preparations at 3.0T during free breathing. Respiratory motion was corrected with a navigator-guided motion correction framework at near perfect efficiency. Image intensities were fit to a mono-exponential function to derive myocardial T_2 maps. The proposed approach (3D-FB-MoCo) was studied in ex-vivo hearts and kidneys, healthy volunteers and canines with acute myocardial infarction (AMI).

Results—Ex-vivo T_2 values from proposed 3D T_2-prep GRE was not different from 2D SE ($p=0.7$) and T_2-prep bSSFP ($p=0.7$). In volunteers, compared to the proposed approach (3D-FB-MoCo) and breath-held 2D T_2-prep bSSFP (2D-BH), non-motion-corrected (3D-FB-Non-MoCo) myocardial T_2 was longer, had larger coefficient-of-variation (COV) and lower image quality (IQ) score (T_2=40.3 ms, COV=38% and IQ=2.3, all $p<0.05$). Conversely, the mean and COV and IQ of 3D-FB-MoCo (T_2=37.7 ms, COV=17% and IQ=3.5.) and 2D-BH (T_2=38.0 ms, COV=15% and IQ=3.8) were not different ($p=0.99$, $p=0.74$, and $p=0.14$, respectively). In AMI, T_2 values and edema volumes from 3D-FB-MoCo and 2D-BH approaches were closely correlated (R^2=0.88 and 0.96, respectively).

Conclusion—The proposed whole-heart T_2 mapping approach can be performed within 5 minutes with similar accuracy to 2D-BH T_2 mapping approach.

Correspondence to: Rohan Dharmakumar, PhD, Dept of Biomedical Sciences, Cedars-Sinai Medical Center, Biomedical Imaging Research Institute, PACT Bldg – Suite 800; 8700 Beverly Blvd, Los Angeles, USA 90048, Phone: (310) 423-7641 | Fax: (310) 248-8682 | rohandkumar@csmc.edu.

[¶]These authors contributed equally to this work

Keywords

fast imaging; cardiac T_2 mapping; myocardial edema; cardiac BOLD MRI

INTRODUCTION

Over the past decade, T_2-based cardiac MRI has evolved as an important tool for characterizing myocardial tissue. To date, numerous clinical and preclinical studies have shown that hyperintensity in T_2 cardiac MRI is associated with myocardial edema, which can be used to stage myocardial infarction (1), detect myocarditis (2), acute ischemia (3) and early transplant rejection (4). Conversely, hypointensity in T_2 MRI has been instrumental in examining intramyocardial hemorrhage (5), chronic iron overloading from ferritin cardiomyopathies (6) (7) and Blood-Oxygen-Level-Dependent (BOLD) MRI (8) (9).

Early approaches typically relied on T_2-weighted imaging (T_2-STIR(1), T_2-prep-SSFP (10,11), etc.), but these approaches have well recognized image artifacts from motion, stagnant/slow moving blood and coil bias (12). As T_2 mapping techniques with high SNR readouts have overcome many of the limitations (3,13,14) and an interest in quantitative tissue characterization became viable and of clinical interest, T_2 mapping has become the preferred means for examining myocardial T_2 changes. (15,16). Nonetheless, to date, T_2 mapping is typically prescribed as 2D breath-held acquisitions to cover the full left ventricle (LV), which takes approximately 10–15 minutes. While respiratory navigator-gated approaches have overcome the discomfort associated with multiple breath holds, the concomitant reduction in scanning efficiency has been a limitation in decreasing the overall scan time to below 10 min (17,18).

In practice, long acquisition time and multiple breath holds impose significant limitations where whole-heart T_2 mapping could be of great value. For instance, in cases where myocardial edema may serve as a marker of acute ischemia in the management of chest pain in the emergency department (19,20), target patients find it difficult to tolerate multiple breath holds and long acquisition times within the scanner. Moreover, in cases where contrast-agent free cardiac stress testing with myocardial BOLD MRI may be valuable, long acquisition times (> 6 minuts) do not permit whole heart T_2 mapping within the standard duration of adenosine infusion (21). The growing interest in T_2-based cardiac MRI for both of these applications could potentially be empowered by a fast, free-breathing T_2 mapping strategy.

Moreover, most T_2 mapping approaches are limited to 1.5T and prescribed with balanced steady-state free precession (bSSFP). Their robustness to image artifacts at 3.0T (banding, B_1 in homogeneity, etc) continues to be problematic (22). A more pragmatic cardiac T_2 mapping approach should be time efficient (preferably < 6 minutes) to accommodate cardiac stress testing with BOLD MRI; enable rapid edema assessment in a clinical environment without suspending breathing ; and should enable reliable acquisitions at 3T with minimal or no image artifacts, while providing full LV coverage. A T_2 mapping technique that conforms to these desirable attributes could enhance rapid assimilation of T_2 imaging as part of time-sensitive and time-efficient clinical cardiac MRI protocols.

We hypothesized that a robust, time-efficient, 3D free-breathing T_2 mapping technique at 3.0T can be obtained through the combined use of (a) adiabatic RF pulses for B_1 insensitive T_2 preparation; (b) near 100% efficient navigator gating with affine motion correction to maximize efficiency of acquisition under free-breathing; and (c) stack-of-stars gradient-echo (GRE) readouts to eliminate banding artifacts associated with bSSFP readouts, without significant loss of SNR. We validated our approach in ex-vivo canine hearts and kidneys, in healthy human volunteers, and in canines subjected to reperfused acute myocardial infarction.

METHODS

Pulse sequence details and data acquisition, motion estimation and correction, and parameter estimation and heart rate corrections pertaining to the proposed imaging approach are described. The motion registration program was written in C using the Insight Toolkit. Image reconstruction and parameter fitting were performed offline using MATLAB (Mathworks, R2009a, MA, USA). All studies were performed on a 3.0 T clinical MRI system (MAGNETOM Verio®, Siemens Healthcare, Erlangen, Germany) and 32 channel matrix coils (16 anterior and 16 posterior) were used for data acquisition.

Pulse Sequence Details and Data Acquisition

A T_2 prepared GRE sequence was adapted for 3D T_2 mapping at 3.0 T. To minimize image artifacts from increased B_0 and B_1 in homogeneities at 3T (23) and cardiac motion, an adiabatic T_2 preparation (2× BIREF-1) (24) was used. A schematic of the timing diagram is shown in Fig. 1 and imaging parameters for each experiment are described in the following section. Images were acquired every other heart beat for longitudinal magnetization recovery. For the GRE readout, we used a stack of slices (along the long axis of the heart) with 144 evenly distributed radial lines to cover the 3D field of view. In each acquisition window (heart beat), a subset of 2–3 in-plane lines from all slices was acquired depending on the length of the quiescent period. In each subset, k-space lines were acquired in a slice-by-slice fashion. Centric reordering along the long axis of the heart was used to minimize T_1 recovery following T_2 preparation and the in-plane radial trajectory was ordered in an interleaved fashion to reduce the possibility of unevenly distributed data in each bin (details on bins below). For example, in a case where two in-plane radial lines A and B are acquired in each subset (A, B), the identity of the pair of radial lines conform to the sequence {(i, i +72)}, where i=1,72 and i is an integer. A representative acquisition scheme with 5 slices and 2 in-plane lines per heartbeat is shown in Fig. 1. GRE readout was trigged at the mid diastolic phase with appropriate trigger delay. A respiratory navigator signal at the lung-liver interface was continually acquired during the free breathing acquisitions without rejecting any data (25). The navigator module was played out before T_2 preparation to (a) avoid potential errors in binning from T_2 weighting of navigator signals at the different TEs; and (b) preserve the T_2 weighting by minimizing T_1 recovery prior to signal readout. In order to derive T_2 maps, the sequence was prescribed with three different T_2 preparation times (TE = 0, 24 and 55 ms).

Motion Estimation and Correction

Motion correction with 3D affine transforms, derived from the respiratory navigator signals, has been shown to reliably correct respiration-mediated motion of the heart (26,27). To maximize imaging efficiency (i.e., utilize all the data acquired during free breathing) the following steps were applied for motion-corrected T_2 mapping:

- *Motion Estimation*:
  - Binning: k-space lines were sorted into 4 bins based on the diaphragm position in which the end expiratory bin was assigned as the reference and the others were labeled as the target bins.
  - Data composition and respiratory phase-resolved image reconstruction: To reduce streaking artifact from undersampling of k-space, composite images were reconstructed by combining the data from all three TEs (within the same respiratory bin) followed by Gaussian smoothing. Representative images acquired at the different TEs for one of the respiratory bins and the effect of combining the images across the different TEs within the same bin are shown in Fig. 2A.
  - Motion Registration: A contour isolating the heart from rest of the anatomy was drawn manually using the 3D image set from the reference bin. The contours were then converted into a mask and applied to images in all respiratory bins. Processed 3D images from each target bin were iteratively registered to the reference bin using Insight Tool Kit (ww.itk.org) (28). Affine transform matrices of each target bin were generated and stored for motion correction. Details of the registration process were previously described by Bhat et al (26).
- *Motion Correction and Image Reconstruction*: k-space data in each respiratory bin were sorted back into independent TEs. After gridding, affine transform matrices were applied to the corresponding images in each respiratory bin and motion-corrected images were reconstructed independently for each TE by combining complex images from all bins. Motion estimation, correction and image reconstruction steps are summarized in Fig. 2B.

Parameter Fitting and Heart Rate Correction

Pixel-wise fitting of signal intensities at the 3 TEs to $a \cdot \exp(-b \cdot TE)$ were performed with log-transformed linear least-squares fit, where a and b are fit parameters with $a = M_0$ (which includes proton density, coil sensitivity etc.) and $b = 1/T_2$. After the fitting for T_2, a heart rate correction was applied to compensate for imperfect T_1 recovery between magnetization preparations. To estimate true T_2, the T_2 estimates from mono-exponential fit ($T_2^{\dagger}$) were multiplied by $(1 + \alpha)$ (Refer to Appendix). α was estimated from known values of T_1 (1100 ms) and T_2 (40 ms) of myocardium, data acquisition in every other heart beat, and ΔTE = 27.5 ms (the midpoint of TEs). Subsequently, heart rate corrected T_2 was calculated as $T_2^{\dagger} \cdot (1 + \alpha)$. If we estimate α assuming T_2 = 40 ms and T_1 = 1200 ms at 3T, then the estimated

errors in α and the corresponding T_2 would be 0.08 ms and 3.2 ms (in cases of significant edema when the actual T_2 = 60 ms and T_1 = 1400 ms) (17,29).

Validation Studies

Ex-vivo Studies—Three freshly excised canine hearts and kidneys were immersed in saline solution and imaged with the proposed method, 2D spin-echo and 2D T_2-prepared bSSFP sequences (with the same adiabatic T_2 preparation as in the proposed method) to assess T_2 accuracy. Proposed 3D sequence was prescribed covering the whole organ and 2D sequences were prescribed to match 3 separated partitions in the organs. Sequences were randomized with regard to order. Imaging parameters of the different sequences were as follows:

- 2D spin echo - TR = 5000 ms, TE = 6, 24, 58 ms, readout bandwidth (BW) = 300 Hz/pixel and voxel size = 2.0 × 2.0 × 6.0 mm^3 interpolated to 1.0 × 1.0 × 3.0 mm^3.
- Proposed 3D T_2 map - GRE readout with stack-of-stars trajectory, TR/TE = 3.4 ms/1.7 ms, flip angle (FA) = 15°, BW = 694 Hz/pixel, 40 lines per heartbeat (simulated heart rate = 60 beats/min), trigger pulse = 2, total projections = 144/slice, field-of-view (FOV) = 380 × 380 mm^2, matrix size = 192 × 192 × 16, and voxel size = 2.0 × 2.0 × 6.0 mm^3 interpolated to 1.0 × 1.0 × 3.0 mm^3, T_2 preparation (as TEs) = 0, 24, 55 ms. Gaussian apodization was used to increase SNR (30).
- 2D T_2 maps with bSSFP readouts with Cartesian trajectory - TR/TE = 2.9 ms/1.1 ms, iPAT = 2, partial Fourier = 3/4, FA = 35°, BW = 1184 Hz/pixel, 86 lines per heartbeat (simulated rate 60/s), trigger pulse = 4, FOV = 288 × 360 mm^2, matrix size = 154 × 192, and voxel size = 2.5 × 1.7 × 6.0 mm^3, T_2 preparation (as TEs) = 0, 24, 55 ms.

Healthy Volunteer Studies—Healthy volunteers (n=10, 3 men, average age 30± 5) were recruited in accordance with the protocol that was reviewed and approved by the Institutional Review Board. Every participant was competent and provided written informed consent and had no history of coronary artery disease, abnormal cardiac rhythm and rate, kidney/liver disease, and were not contraindicated for cardiac MR exams (completed a detailed cardiac MRI questionnaire). All studies were performed on the same clinical MRI system used for ex vivo studies with subjects placed on the supine position. After whole heart shimming and localization, proposed free-breathing 3D T_2-prepared acquisitions were prescribed with whole LV coverage using 25% slice over-sampling and 32–48 radial lines per heartbeat triggered at approximately mid-diastole within a data acquisition window of 110–160 ms. A four-chamber cine scan was used to determine the quiescent period of the cardiac cycle. Navigator pulses were placed on the dome of the right hemidiaphragm. The data was reconstructed as described earlier to generate T_2 maps. For comparison purposes, images were also reconstructed without motion correction. Also, the standard 2D breath-held T_2-prepared bSSFP acquisitions were prescribed along representative short-axis slices that were matched to three slices centered at the level of mid ventricle within the 3D partitions. Imaging parameters and T_2-preparation schemes were the same as those used for

ex-vivo imaging. To minimize bias with respect to acquisition order, the acquisitions were randomized.

Canine Model of Acute Myocardial Infarction—Dogs (*n*= 10, 18–26 kg) were studied according to the protocols approved by the Institutional Animal Care and Use Committee. Animals were anesthetized, intubated and mechanically ventilated with 100% O_2 mixed with isoflurane (1.0–2.5%). Subsequently, the dogs underwent left thoracotomies and the left anterior descending artery was ligated at 1.0–1.5 cm from the bifurcation of the left main coronary artery for 3 hours followed by reperfusion. The dogs were allowed to recover for 4 days before imaging studies.

Prior to imaging, animals were fasted, sedated, anesthetized, intubated, and transferred to the scanner table and were mechanically ventilated via a pneumatic anesthesia ventilator. Subsequently, they were placed on the scanner table in the feet-first right-lateral position. The imaging protocol (localizations, cardiac shimming, and T_2-weighted acquisitions) and the scan parameters of proposed free-breathing 3D T_2-prepared acquisitions were the same as those used for the human studies except for the FOV, number of slices acquired, and acquisition window (95–140 ms) reduced to adjust for differences in cardiac dimension and heart rate. 2D breath-held T_2-prepared bSSFP acquisitions and phase-sensitive inversion recovery (PSIR) late-gadolinium-enhancement (LGE) acquisitions were prescribed with full left ventricle coverage comprising slices matched to the 3D partitions. PSIR LGE images were acquired 10 minutes after Gd-DTPA infusion (0.2 mmol/kg, gadoversetamide/ Optimark, Mallinckrodt Inc., Hazelwood, MO), using non-selective inversion recovery preparation with GRE readout (TR/TE = 3.2/1.5 ms, FA = 20°, BW = 586 Hz/pixel, matrix = 96 × 192, in-plane resolution = 1.3 × 1.3 mm^2; and slice thickness = 6.0 mm). A TI-scout sequence was used to find the optimal TI for nulling the healthy myocardium (240–270 ms).

Image Analysis and Statistics

All reconstructed T_2 maps were analyzed in cvi[42] (Circle Cardiovascular Imaging Inc., Calgary, AB, Canada). Images were imported into cvi[42] and endo- and epi-cardial contours were drawn to segment the myocardium for further T_2 analysis. In addition, all statistical analyses were performed in IBM SPSS (V21.0, NY, USA).

Ex vivo Studies—After segmenting the myocardium and parenchyma of the kidney, mean T_2 values of the organs determined from images acquired using 2D spin echo, 2D T_2-prepared bSSFP and 3D T_2-prepared (proposed) sequences were compared. Repeated measurements ANOVA tests were performed to examine whether the T_2 values were different between different sequences. Post-hoc comparison with Bonferroni correction was used if the null hypothesis was rejected.

Human Studies—The mean and coefficient-of-variation (COV) of myocardial T_2, as well as overall image quality scores of the T_2 maps generated using images from the (i) proposed 3D sequence with motion correction (3D FB MoCo), (ii) proposed 3D sequence without motion correction (3D FB Non-MoCo, using all respiratory phases), and (iii) 2D breath-held sequence (2D BH) were measured. Two independent, experienced observers who were

blinded to the acquisition details evaluated image quality. All image quality assessments were based on the T_2 maps. Mean myocardial T_2 values were measured from the segmented myocardium and the COV of T_2 was calculated as the quotient of the mean T_2 and the corresponding standard deviation. Image quality was graded as 1, poor (non assessable); 2, fair (mild to moderate artifacts); 3, good (minimal to mild artifacts); 4, excellent (minimal or no artifacts). Repeated measurements ANOVA tests (mean T_2 and COV in T_2) and Friedman test (image quality scores) were performed to examine whether the measures were different between the three techniques. Post-hoc comparison with Bonferroni correction was used if the null hypothesis was rejected.

Canine Studies—Following segmentation of the myocardium (as described earlier), remote myocardium was defined as the region showing no hyperintensity on LGE images. A reference region of interest was drawn in remote myocardium on both LGE images and copied onto the corresponding slice positions of 2D and 3D T_2 maps. Affected myocardium was defined as the hyperintense region with mean signal intensity at least 2 standard deviations (SDs) above that of the reference region of interest on both 2D and 3D T_2 maps (13). Only LGE positive imaging slices were included in the analysis. Regression analysis was performed between slice-matched 2D and 3D acquisitions for (a) mean T_2 values of remote and affected (edematous) myocardium; and (b) % edema volume, defined as the relative volume of affected myocardium to the total volume of the myocardium on a per-slice basis, for all animals. Bland-Altman analysis was performed to examine the limits of agreement and bias in mean T_2 and % edema volume between the proposed 3D approach and the 2D approach.

RESULTS

Ex vivo Studies

Representative T_2 maps obtained using 2D spin-echo and T_2-prep bSSFP acquisitions along with the proposed 3D acquisition (matched to the 2D slice) are shown in Fig. 3A. Mean T_2 values derived from each sequences are shown in Fig. 3B (2D spin-echo T_2 = 40.8±2.4 ms (heart), 52.4±0.5 ms (kidney) ms; 2D T_2-prep bSSFP T_2 = 42.4±1.6 (heart), 52.9±1.1 (kidney) ms; and proposed 3D sequence T_2 = 40.2±2.5 (Heart), 51.3±0.7 (kidney) ms). Relative to the “gold standard” T_2 values (2D spin-echo), T_2 values obtained with 2D T_2-prep bSSFP and 3D T_2-prep GRE were not different ($p = 0.7$ and $p=0.2$, respectively).

Healthy Volunteers

Figure 4 shows representative slice-matched T_2-weighted images (Fig. 4A) and T_2 maps (Fig. 4B) obtained using 3D FB MoCo, 3D FB Non-MoCo, and 2D BH approaches. 2D BH and 3D FB MoCo images at the different TEs appeared to have comparable image quality, while image blurring from respiratory motion was evident in 3D FB Non-MoCo images and maps (arrows). Quantitative measures of agreement between the methods are shown in Fig. 5 and collected in Table 1. 3D FB Non-MoCo showed significantly greater COV ($p<0.05$), longer T_2 values ($p<0.05$), and lower IQ ($p<0.05$) compared to 3D FB MoCo and 2D BH images and maps. Conversely, 2D BH and 3D FB MoCo approaches did not show differences in mean T_2 ($p=0.99$), COV T_2 ($p=0.74$), and IQ ($p=0.14$).

Canines with Reperfused Acute Myocardial Infarction

Representative slice-matched images (Fig. 6A) and T_2-maps (Fig. 6B) obtained with the proposed 3D FB MoCo and 2D BH obtained on day 4 post-MI are shown. Corresponding LGE images are also shown for visual confirmation for the presence of infarction in the LAD territory. Edema (and infarction) was identified in 2–4 short-axis slices in each of the animals. Close correspondence between edematous territories in the slice-matched 2D BH and 3D FB T_2 maps, and the enhanced territories in LGE images was observed. T_2 values were significantly elevated in regions positive for LGE in both 2D BH and 3D FB T_2 maps. Linear regression analysis showed that the T_2 estimates (edematous and remote territories) and the % edema volume measured from 2D BH and 3D FB MoCo T_2 maps were closely correlated (R^2 = 0.88,and 0.96, respectively. Both $p<0.05$). Bland-Altman plots of mean T_2 measures from edematous territories and remote myocardium and % Edema Volume were within the limits of agreement (bias in T_2 = 0.4 ms; bias in % Edema Volume = 0.9%). The edema and LGE positive territories (on per slices basis) agreed well (R^2 = 0.8, $p<0.05$) with the edema volume have a positive bias of 8% over LGE volume.

DISCUSSION

In this study we successfully developed and tested a motion-corrected, free-breathing 3D T_2 mapping technique using GRE-based stack-of-stars acquisition at 3T that can be completed within 5 minutes. The accuracy of T_2 measures from motion-corrected reconstruction was examined in ex-vivo canine hearts and kidneys, healthy human volunteers, and controlled canine model of acute myocardial infarction, respectively. The results showed that compared to the commonly used T_2 mapping approach (2D acquisitions with multiple breath holds), the proposed 3D T_2 mapping strategy can reliably estimate T_2 values of the myocardium in health and disease. The proposed method is expected to be beneficial in patients who cannot tolerate suspension of breathing and in cases where the imaging exam needs to be completed with whole heart coverage within a short period of time. Hence the key features of the proposed approach (free-breathing, full LV coverage coverage and fast acquisitions) are expected to be particularly valuable in the management of chest pain in emergency department where myocardial edema may be used as a marker of ongoing ischemia (3) and for contrast-free cardiac stress testing using myocardial BOLD MRI (8,9).

While the benefits of fast, free-breathing T_2 mapping of whole LV over the conventional multiple-breath-held T_2 mapping are clear, it is useful to contrast the proposed approach against previously proposed 3D T_2 mapping approaches. While navigator gated methods have shown low imaging efficiency and residual motion artifacts, different methods have been proposed to correct for respiratory motion and accelerate acquisition (17,31). In particular, the recent development by Heeswijk, et al. (31) has markedly reduced acquisition time. However, since their T_2 mapping approach is founded upon 3D high-resolution isotropic imaging, acquisition time continues to be near 20 minutes, which imposes limitations on its use for time sensitive applications discussed above.

In this study we utilized a 3D stack-of-stars sampling scheme for T_2 mapping, which lends some key benefits. First, at a heart rate of 60 beats/minute, with 48 projections acquired every other heartbeat, the total acquisition time for whole LV coverage is less than 5

minutes. Since the proposed approach does not restrict one to isotropic resolution, it provides the flexibility to control the resolution along the long axis, and hence imaging time, depending on the needs of the study. Second, the proposed approach allows for centric encoding, which reduces the T_1 dependency in T_2 maps (17). Finally, the proposed T_2 mapping strategy offers robust image quality at 3T since the proposed approach uses adiabatic T_2 preparation combined with GRE readouts to overcome image artifacts from B_1 and B_0 in homogeneities at 3T. Although bSSFP readouts can provide significant signal-to-noise benefits over GRE, previous studies have shown insignificant differences in myocardial T_2 between the two readout sequences at 1.5T (32). Consistent with these studies, in the current study at 3T we observed comparable COV in myocardial T_2 between bSSFP and GRE readout schemes. Nonetheless both readout schemes have their limitations in extreme cases - GRE acquisitions can suffer from lower SNR and have less homogeneous signal in large patients; and bSSFP readouts are prone to unavoidable banding artifacts.

The T_2 values measured under conditions of health in this study were comparable to the values previously reported in humans. Specifically, we found that the T_2 value of the healthy myocardium to be 37.7±2.0 ms vs. 38.5 ± 4.5 ms (17). Similar observations were made in animals with acute myocardial infarction as well (T_2 in the infarct zone from our study was 55.2±7.1 ms vs. 58.1 ± 6.9 ms (33) and T_2 in remote zone from our study was 36.7±3.5 ms vs. 41.1 ± 5.2 ms (33)). These favorable comparisons between our results and those reported in the literature further confirm that the proposed technique is a reliable method for measuring myocardial T_2 under conditions of health and disease.

Although not explored here, we anticipate that further shortening of scan time may be possible using parallel imaging techniques (34,35) and/or compressed sensing (36) schemes. However, to avoid potential “smoothing” artifacts observed in certain accelerated approaches and also to strictly examine the capability of motion correction, we did not consider any imaging acceleration techniques in the current study. Additional studies are necessary to examine the limits of imaging acceleration strategies within the constraints of reliable measurements of myocardial T_2.

There were some limitations in this study. First, while this study employed ex-vivo and in-vivo preparations of animals and healthy volunteers and showed that the proposed 3D approach can yield similar values of T_2 as 2D breath-held acquisitions, the sample size of the study is limited. Additional studies are required to assess the robustness of the method under various physiological conditions, particularly in human subjects with disease. Second, based on the mono exponential model, 3 TEs are the minimum requirement for a least-squares linear-regression fitting of the logarithmically transformed data. To map the T_2 of the remote and affected myocardium, we set the latest TE to be 55 ms, so as to achieve a reasonable dynamic range in signal intensities for the affected territory (which tends to have T_2 ~ 60 ms) and still have sufficient in the remote myocardium (T_2 ~ 40 ms). Although additional TEs may improve robustness of T_2 fits (37), extra acquisition time associated with greater number of TEs can extend the study time beyond the demands of the key applications outlined earlier. Based on comparable results we obtained here in relation to past work (4,13,14,17,38), we expect that three TEs to be a good tradeoff between imaging speed and fidelity of myocardial T_2 fits under conditions of health and disease. Third, in this

study we assumed that the prescribed slice positions between 2D and 3D acquisition are the same, which may not be the case. To minimize this error, the data in the reference bin was always acquired at end expiration. Also, given that 2D slice thickness and 3D partitions are similar (6 mm), we anticipate that any contributions from potential differences to be small. Moreover, we used only 4 bins to derive and correct for respiration-induced motion. Previous studies that employed affine motion correction on the raw data (26,39) used 6 bins to estimate respiration-mediated motion for coronary MR angiography. Finally, we estimated the correction term (α) based on known T_1 and T_2 values of the myocardium at 3T in health. Since T_1 and T_2 of the edematous myocardium can be greater than 30% and 50% of the normal myocardium (17,29), respectively, it is conceivable that α may not be accurately estimated on the basis of healthy myocardial T_1 and T_2 values. However, our calculations showed that even in the presence of significant edema (T_1 =1400 ms, T_2=60 ms), the estimated error in α determined using healthy T_1=1200 ms and T_2=40 ms values is within 8%, which corresponds to a deviation in T_2 of 3.2 ms, which is comparable to the standard deviation of myocardial T_2.

Nonetheless, the results here suggest that the quality of motion correction based on the empirical binning at reduced resolution is adequate for reliable estimation of myocardial T_2 values under conditions of health and disease.

CONCLUSION

We developed and tested a free-breathing 3D T_2 mapping approach at 3T with respiratory motion correction, which can be performed within 5 minutes. The proposed approach yielded accurate estimates of myocardial T_2 in explanted canine hearts and kidneys, healthy human volunteers, and canines with reperfused acute myocardial infarction. Clinical studies are needed to validate the robustness of the proposed approach in patients.

Acknowledgments

FUNDING INFORMATION

This work was supported in part by National Heart, Lung, and Blood Institute HL091989 (R.D.) and American Heart Association Grants 14SDG20480123 (B.S.) and 13PRE17210049 (A.K). The content is solely the responsibility of the authors and does not necessarily represent the official views of the American Heart Association or the National Heart, Lung, And Blood Institute or the National Institutes of Health.

APPENDIX

In the centric encoding scheme, the longitudinal magnetization immediately following T_2 preparation of each heart beat can be written iteratively as

$$M_{T2+} = (M_0 + (M_{T2-} - M_0)E_1)E_{2TE}, \quad (1)$$

where M_{T2+} and M_{T2-} are longitudinal magnetizations following the T_2 preparations in the recent (M_{T2+}) and previous (M_{T2-}) heart beats, M_0 is magnetization at thermal equilibrium, $E_1=\exp(-RT/T_1)$ with RT = recovery time, and $E_{2TE}= \exp(-TE/T_2)$. Assuming heart rate is constant throughout the acquisition, M_{T2} term will reach a steady state after a few heart beats (i.e. $M_{T2+} = M_{T2-} = M_{T2}$) and (1) can be rearranged to get

$$M_{T2}=\frac{E_{2TE}M_0(1-E_1)}{(1-E_1E_{2TE})} \quad (2)$$

and the acquired signal can be expressed as

$$S_{TE}=GM_{T2} \quad (3)$$

G accounts for readout scheme, coil sensitivity, etc.

When RT >> T_1, $E_1 \sim 0$, R_2 (or $1/T_2$) can be derived with 2 measurements with different TEs using

$$\log\left(\frac{S_{TE1}}{S_{TE2}}\right)=\Delta TER_2, \quad (4)$$

where ΔTE = TE1 − TE2. However when RT is comparable to T_1, E_1 is not negligible and (2) has to be rewritten as

$$\log\left(\frac{S_{TE1}}{S_{TE2}}\right)=\Delta TE\cdot R_2^{\dagger}, \quad (5)$$

$$\text{where} R_2^{\dagger}=R_2(1+\alpha), \text{with}\alpha=\frac{\log(\frac{1-E_1E_{2TE2}}{1-E_1E_{2TE1}})}{R_2\Delta TE} \quad (6)$$

S_{TE1}, S_{TE2}, are Image intensities corresponding to the first and second TE and αR_2 is the bias in R_2 estimated from fitting to a mono-exponential under the assumption of perfect T_1 recovery $(R_2^{\dagger})$. Hence the appropriate correction factor to estimate true T_2 is (1 + α); that is $T_2=T_2^{\dagger}(1+\alpha)$, where $T_2^{\dagger}$ is $1/R_2^{\dagger}$.

REFERENCES

1. Abdel-Aty H, Zagrosek A, Schulz-Menger J, Taylor AJ, Messroghli D, Kumar A, Gross M, Dietz R, Friedrich MG. Delayed enhancement and T2-weighted cardiovascular magnetic resonance imaging differentiate acute from chronic myocardial infarction. Circulation. 2004; 109(20):2411–2416. [PubMed: 15123531]
2. Friedrich MG, Sechtem U, Schulz-Menger J, Holmvang G, Alakija P, Cooper LT, White JA, Abdel-Aty H, Gutberlet M, Prasad S, Aletras A, Laissy JP, Paterson I, Filipchuk NG, Kumar A, Pauschinger M, Liu P. International Consensus Group on Cardiovascular Magnetic Resonance in M. Cardiovascular magnetic resonance in myocarditis: A JACC White Paper. Journal of the American College of Cardiology. 2009; 53(17):1475–1487. [PubMed: 19389557]
3. Verhaert D, Thavendiranathan P, Giri S, Mihai G, Rajagopalan S, Simonetti OP, Raman SV. Direct T2 quantification of myocardial edema in acute ischemic injury. JACC Cardiovascular imaging. 2011; 4(3):269–278. [PubMed: 21414575]
4. Usman AA, Taimen K, Wasielewski M, McDonald J, Shah S, Giri S, Cotts W, McGee E, Gordon R, Collins JD, Markl M, Carr JC. Cardiac magnetic resonance T2 mapping in the monitoring and follow-up of acute cardiac transplant rejection: a pilot study. Circulation Cardiovascular imaging. 2012; 5(6):782–790. [PubMed: 23071145]
5. Payne AR, Casey M, McClure J, McGeoch R, Murphy A, Woodward R, Saul A, Bi X, Zuehlsdorff S, Oldroyd KG, Tzemos N, Berry C. Bright-blood T2-weighted MRI has higher diagnostic accuracy

than dark-blood short tau inversion recovery MRI for detection of acute myocardial infarction and for assessment of the ischemic area at risk and myocardial salvage. Circulation Cardiovascular imaging. 2011; 4(3):210–219. [PubMed: 21427362]

6. He T, Gatehouse PD, Smith GC, Mohiaddin RH, Pennell DJ, Firmin DN. Myocardial T2* measurements in iron-overloaded thalassemia: An in vivo study to investigate optimal methods of quantification. Magnetic resonance in medicine : official journal of the Society of Magnetic Resonance in Medicine/Society of Magnetic Resonance in Medicine. 2008; 60(5):1082–1089.
7. Papanikolaou N, Ghiatas A, Kattamis A, Ladis C, Kritikos N, Kattamis C. Non-invasive myocardial iron assessment in thalassaemic patients. T2 relaxometry and magnetization transfer ratio measurements. Acta radiologica. 2000; 41(4):348–351. [PubMed: 10937756]
8. Fieno DS, Shea SM, Li Y, Harris KR, Finn JP, Li D. Myocardial perfusion imaging based on the blood oxygen level-dependent effect using T2-prepared steady-state free-precession magnetic resonance imaging. Circulation. 2004; 110(10):1284–1290. [PubMed: 15326062]
9. Arnold JR, Karamitsos TD, Bhamra-Ariza P, Francis JM, Searle N, Robson MD, Howells RK, Choudhury RP, Rimoldi OE, Camici PG, Banning AP, Neubauer S, Jerosch-Herold M, Selvanayagam JB. Myocardial oxygenation in coronary artery disease: insights from blood oxygen level-dependent magnetic resonance imaging at 3 tesla. Journal of the American College of Cardiology. 2012; 59(22):1954–1964. [PubMed: 22624835]
10. Shea SM, Fieno DS, Schirf BE, Bi X, Huang J, Omary RA, Li D. T2-prepared steady-state free precession blood oxygen level-dependent MR imaging of myocardial perfusion in a dog stenosis model. Radiology. 2005; 236(2):503–509. [PubMed: 16040907]
11. Kellman P, Aletras AH, Mancini C, McVeigh ER, Arai AE. T2-prepared SSFP improves diagnostic confidence in edema imaging in acute myocardial infarction compared to turbo spin echo. Magnetic resonance in medicine : official journal of the Society of Magnetic Resonance in Medicine/Society of Magnetic Resonance in Medicine. 2007; 57(5):891–897.
12. Abdel-Aty H, Simonetti O, Friedrich MG. T2-weighted cardiovascular magnetic resonance imaging. Journal of magnetic resonance imaging : JMRI. 2007; 26(3):452–459. [PubMed: 17729358]
13. Giri S, Chung YC, Merchant A, Mihai G, Rajagopalan S, Raman SV, Simonetti OP. T2 quantification for improved detection of myocardial edema. Journal of cardiovascular magnetic resonance : official journal of the Society for Cardiovascular Magnetic Resonance. 2009; 11:56. [PubMed: 20042111]
14. Thavendiranathan P, Walls M, Giri S, Verhaert D, Rajagopalan S, Moore S, Simonetti OP, Raman SV. Improved detection of myocardial involvement in acute inflammatory cardiomyopathies using T2 mapping. Circulation Cardiovascular imaging. 2012; 5(1):102–110. [PubMed: 22038988]
15. He T, Gatehouse PD, Anderson LJ, Tanner M, Keegan J, Pennell DJ, Firmin DN. Development of a novel optimized breathhold technique for myocardial T2 measurement in thalassemia. Journal of magnetic resonance imaging : JMRI. 2006; 24(3):580–585. [PubMed: 16892203]
16. Guo H, Au WY, Cheung JS, Kim D, Jensen JH, Khong PL, Chan Q, Chan KC, Tosti C, Tang H, Brown TR, Lam WW, Ha SY, Brittenham GM, Wu EX. Myocardial T2 quantitation in patients with iron overload at 3 Tesla. Journal of magnetic resonance imaging : JMRI. 2009; 30(2):394–400. [PubMed: 19629983]
17. van Heeswijk RB, Feliciano H, Bongard C, Bonanno G, Coppo S, Lauriers N, Locca D, Schwitter J, Stuber M. Free-breathing 3 T magnetic resonance T2-mapping of the heart. JACC Cardiovascular imaging. 2012; 5(12):1231–1239. [PubMed: 23236973]
18. Giri S, Shah S, Xue H, Chung YC, Pennell ML, Guehring J, Zuehlsdorff S, Raman SV, Simonetti OP. Myocardial T(2) mapping with respiratory navigator and automatic nonrigid motion correction. Magnetic resonance in medicine : official journal of the Society of Magnetic Resonance in Medicine/Society of Magnetic Resonance in Medicine. 2012; 68(5):1570–1578.
19. Raman SV, Simonetti OP, Winner MW 3rd, Dickerson JA, He X, Mazzaferri EL Jr, Ambrosio G. Cardiac magnetic resonance with edema imaging identifies myocardium at risk and predicts worse outcome in patients with non-ST-segment elevation acute coronary syndrome. Journal of the American College of Cardiology. 2010; 55(22):2480–2488. [PubMed: 20510215]

20. Abdel-Aty H, Cocker M, Meek C, Tyberg JV, Friedrich MG. Edema as a very early marker for acute myocardial ischemia: a cardiovascular magnetic resonance study. Journal of the American College of Cardiology. 2009; 53(14):1194–1201. [PubMed: 19341860]
21. Gerber BL, Raman SV, Nayak K, Epstein FH, Ferreira P, Axel L, Kraitchman DL. Myocardial first-pass perfusion cardiovascular magnetic resonance: history, theory, and current state of the art. Journal of cardiovascular magnetic resonance : official journal of the Society for Cardiovascular Magnetic Resonance. 2008; 10:18. [PubMed: 18442372]
22. Schar M, Kozerke S, Fischer SE, Boesiger P. Cardiac SSFP imaging at 3 Tesla. Magnetic resonance in medicine : official journal of the Society of Magnetic Resonance in Medicine/Society of Magnetic Resonance in Medicine. 2004; 51(4):799–806.
23. Nezafat R, Stuber M, Ouwerkerk R, Gharib AM, Desai MY, Pettigrew RI. B1-insensitive T2 preparation for improved coronary magnetic resonance angiography at 3 T. Magnetic resonance in medicine : official journal of the Society of Magnetic Resonance in Medicine/Society of Magnetic Resonance in Medicine. 2006; 55(4):858–864.
24. Jenista ER, Rehwald WG, Chen EL, Kim HW, Klem I, Parker MA, Kim RJ. Motion and flow insensitive adiabatic T2 -preparation module for cardiac MR imaging at 3 Tesla. Magnetic resonance in medicine : official journal of the Society of Magnetic Resonance in Medicine/Society of Magnetic Resonance in Medicine. 2013; 70(5):1360–1368.
25. Stuber M, Botnar RM, Danias PG, Kissinger KV, Manning WJ. Submillimeter three-dimensional coronary MR angiography with real-time navigator correction: comparison of navigator locations. Radiology. 1999; 212(2):579–587. [PubMed: 10429721]
26. Bhat H, Ge L, Nielles-Vallespin S, Zuehlsdorff S, Li D. 3D radial sampling and 3D affine transform-based respiratory motion correction technique for free-breathing whole-heart coronary MRA with 100% imaging efficiency. Magnetic resonance in medicine : official journal of the Society of Magnetic Resonance in Medicine/Society of Magnetic Resonance in Medicine. 2011; 65(5):1269–1277.
27. Manke D, Nehrke K, Bornert P. Novel prospective respiratory motion correction approach for free-breathing coronary MR angiography using a patient-adapted affine motion model. Magnetic resonance in medicine : official journal of the Society of Magnetic Resonance in Medicine/Society of Magnetic Resonance in Medicine. 2003; 50(1):122–131.
28. Luis, ISW.; Ng, L.; Cates, J. the Insight Software Consortium, (www.itk.org). The ITK Software Guide. 2nd Ed.. 2005. Updated for ITK version 2.4. 2.4;
29. Kali A, Cokic I, Tang RL, Yang HJ, Sharif B, Marban E, Li D, Berman DS, Dharmakumar R. Determination of location, size, and transmurality of chronic myocardial infarction without exogenous contrast media by using cardiac magnetic resonance imaging at 3 T. Circulation Cardiovascular imaging. 2014; 7(3):471–481. [PubMed: 24682268]
30. Sharif B, Dharmakumar R, Arsanjani R, Thomson L, Bairey Merz CN, Berman DS, Li D. Non-ECG-gated myocardial perfusion MRI using continuous magnetization-driven radial sampling. Magnetic resonance in medicine : official journal of the Society of Magnetic Resonance in Medicine/Society of Magnetic Resonance in Medicine. 2014 10.100/mrm25074.
31. van Heeswijk RB, Piccini D, Feliciano H, Hullin R, Schwitter J, Stuber M. Self-navigated isotropic three-dimensional cardiac T2 mapping. Magnetic resonance in medicine : official journal of the Society of Magnetic Resonance in Medicine/Society of Magnetic Resonance in Medicine. 2014 10.1002/mrm.25258.
32. Wassmuth R, Prothmann M, Utz W, Dieringer M, von Knobelsdorff-Brenkenhoff F, Greiser A, Schulz-Menger J. Variability and homogeneity of cardiovascular magnetic resonance myocardial T2-mapping in volunteers compared to patients with edema. Journal of cardiovascular magnetic resonance : official journal of the Society for Cardiovascular Magnetic Resonance. 2013; 15:27. [PubMed: 23537111]
33. Ghugre NR, Pop M, Barry J, Connelly KA, Wright GA. Quantitative magnetic resonance imaging can distinguish remodeling mechanisms after acute myocardial infarction based on the severity of ischemic insult. Magnetic resonance in medicine : official journal of the Society of Magnetic Resonance in Medicine/Society of Magnetic Resonance in Medicine. 2013; 70(4):1095–1105.
34. Pang J, Sharif B, Arsanjani R, Bi X, Fan Z, Yang Q, Li K, Berman DS, Li D. Accelerated whole-heart coronary MRA using motion-corrected sensitivity encoding with three-dimensional

projection reconstruction. Magnetic resonance in medicine : official journal of the Society of Magnetic Resonance in Medicine/Society of Magnetic Resonance in Medicine. 2014; 71(1):67–74.

35. Wright KL, Hamilton JI, Griswold MA, Gulani V, Seiberlich N. Non-Cartesian parallel imaging reconstruction. Journal of magnetic resonance imaging : JMRI. 2014 Nov; 40(5):1022–1040. [PubMed: 24408499]
36. Doneva M, Bornert P, Eggers H, Stehning C, Senegas J, Mertins A. Compressed sensing reconstruction for magnetic resonance parameter mapping. Magnetic resonance in medicine : official journal of the Society of Magnetic Resonance in Medicine/Society of Magnetic Resonance in Medicine. 2010; 64(4):1114–1120.
37. MacFall JR, Riederer SJ, Wang HZ. An analysis of noise propagation in computed T2, pseudodensity, and synthetic spin-echo images. Medical physics. 1986; 13(3):285–292. [PubMed: 3724687]
38. von Knobelsdorff-Brenkenhoff F, Prothmann M, Dieringer MA, Wassmuth R, Greiser A, Schwenke C, Niendorf T, Schulz-Menger J. Myocardial T1 and T2 mapping at 3 T: reference values, influencing factors and implications. Journal of cardiovascular magnetic resonance : official journal of the Society for Cardiovascular Magnetic Resonance. 2013; 15:53. [PubMed: 23777327]
39. Pang J, Bhat H, Sharif B, Fan Z, Thomson LE, LaBounty T, Friedman JD, Min J, Berman DS, Li D. Whole-heart coronary MRA with 100% respiratory gating efficiency: self-navigated three-dimensional retrospective image-based motion correction (TRIM). Magnetic resonance in medicine : official journal of the Society of Magnetic Resonance in Medicine/Society of Magnetic Resonance in Medicine. 2014; 71(1):67–74.

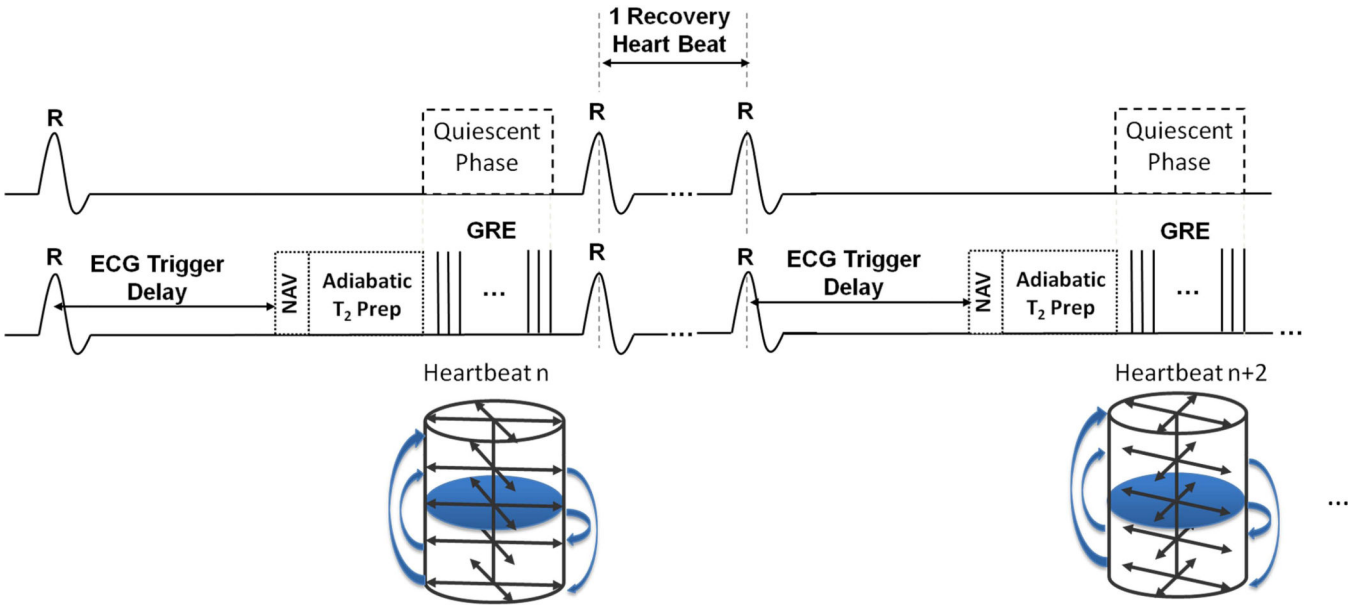

Fig. 1. Pulse sequence timing diagram and k-space trajectory

Details of the pulse sequence and the relative timing are presented in panels A and B. GRE readout is triggered during the quiescent period at mid diastole with a proper trigger delay from the R wave. Panel C shows an example of the stack-of-stars trajectory with 2 radial lines in each subset and 5 partitions.

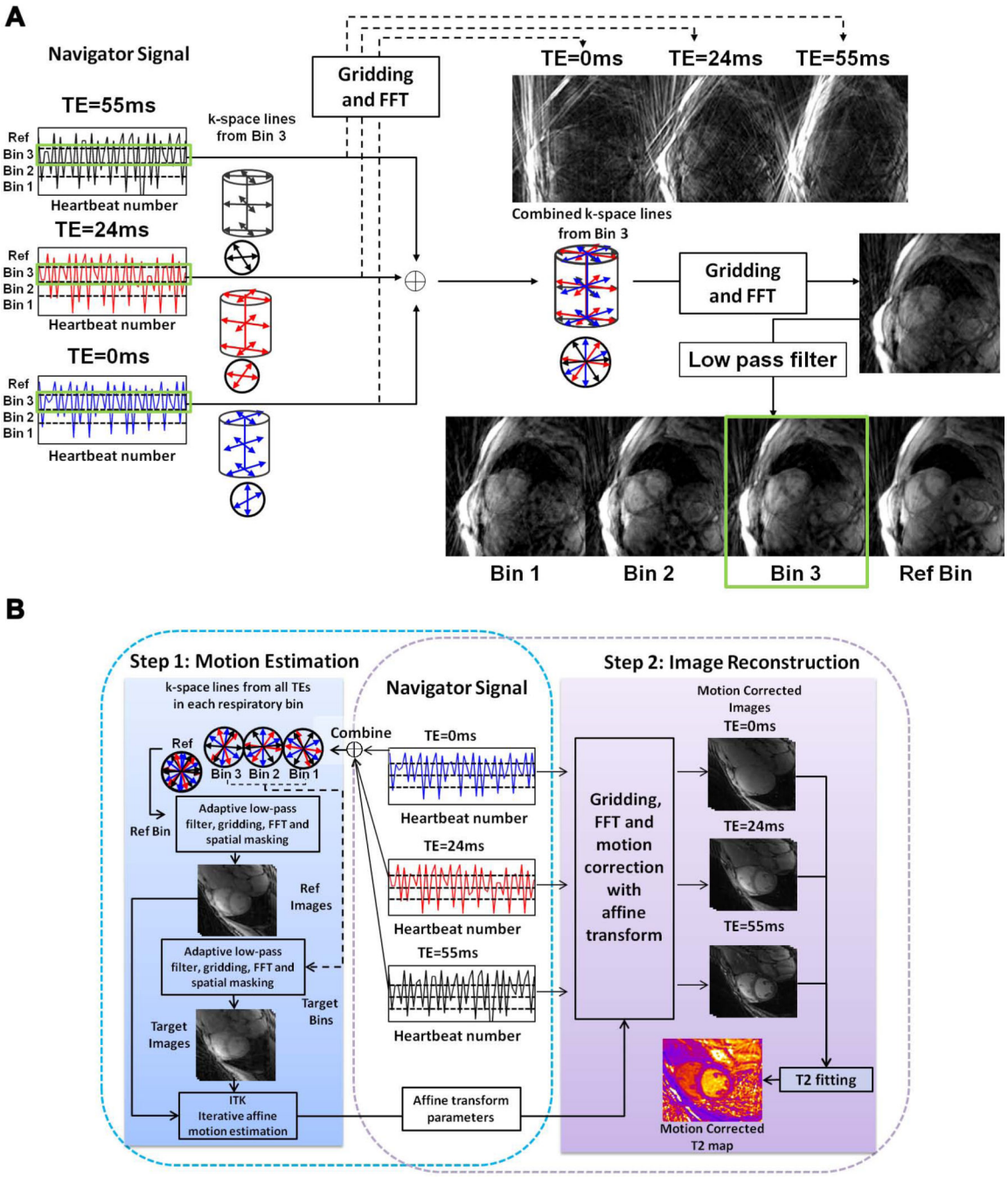

Fig. 2. Image reconstruction steps

Panel A shows a representative case of combining undersampled low-resolution images from a common respiratory phase from different TEs to arrive at composite data sets for each bin. This is shown for Bin 3 here. Similar steps are taken to arrive at data for Bins 1, 2 and reference bin (Ref Bin, end expiratory phase). Panel B shows the steps associated with motion correction (binning based on navigator signal, estimation of motion and image reconstruction) and parameter fitting. In essence, the k-space data is first combined with different TEs and separated into different respiratory bins based on the navigator signal.

From each bin, a low-resolution composite image representing different respiratory position was reconstructed. On the basis of the reference bin, the affine motion parameters of all other (target) bins were estimated with ITK and stored for motion correction. Finally, k-space data with different T_2 preparations were gridded independently and applied with corresponding affine transformation to yield motion-corrected images. Subsequently the pixel-wise fitting is performed using the images at different TEs to estimate T_2.

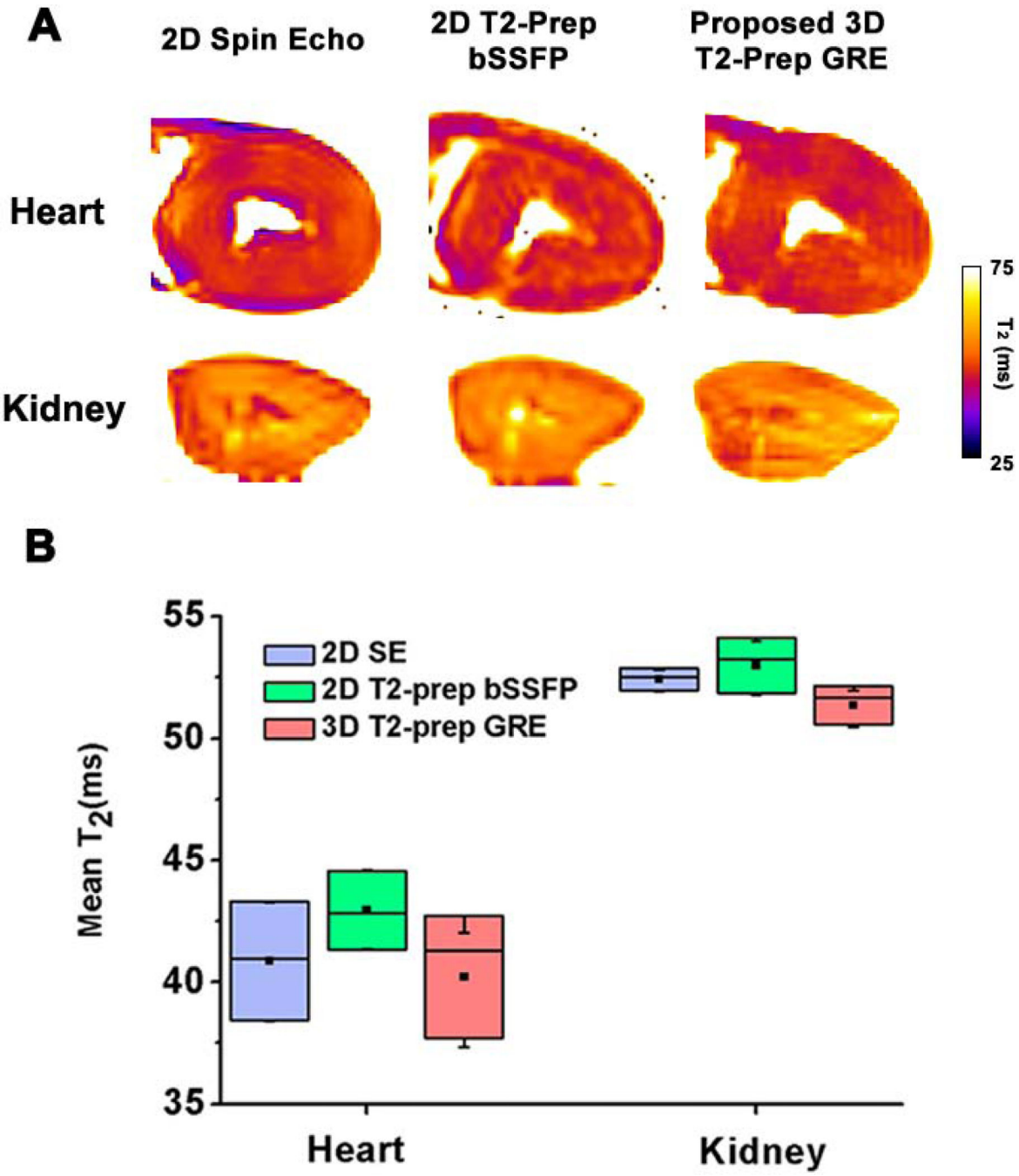

Fig. 3. Representative short-axis T_2 maps and box-plot of mean myocardial T_2 from explanted dog hearts and kidneys obtained with 2D spin echo, 2D T_2-prep SSFP and 3D T_2-prep GRE acquisitions

(A) Slice-matched T_2 maps obtained at the level of mid ventricle from an explanted dog heart and mid slice of dog kidney using the different T_2 approaches are shown. Mean T_2 values (B) between the approaches were not different for heart and kidney.

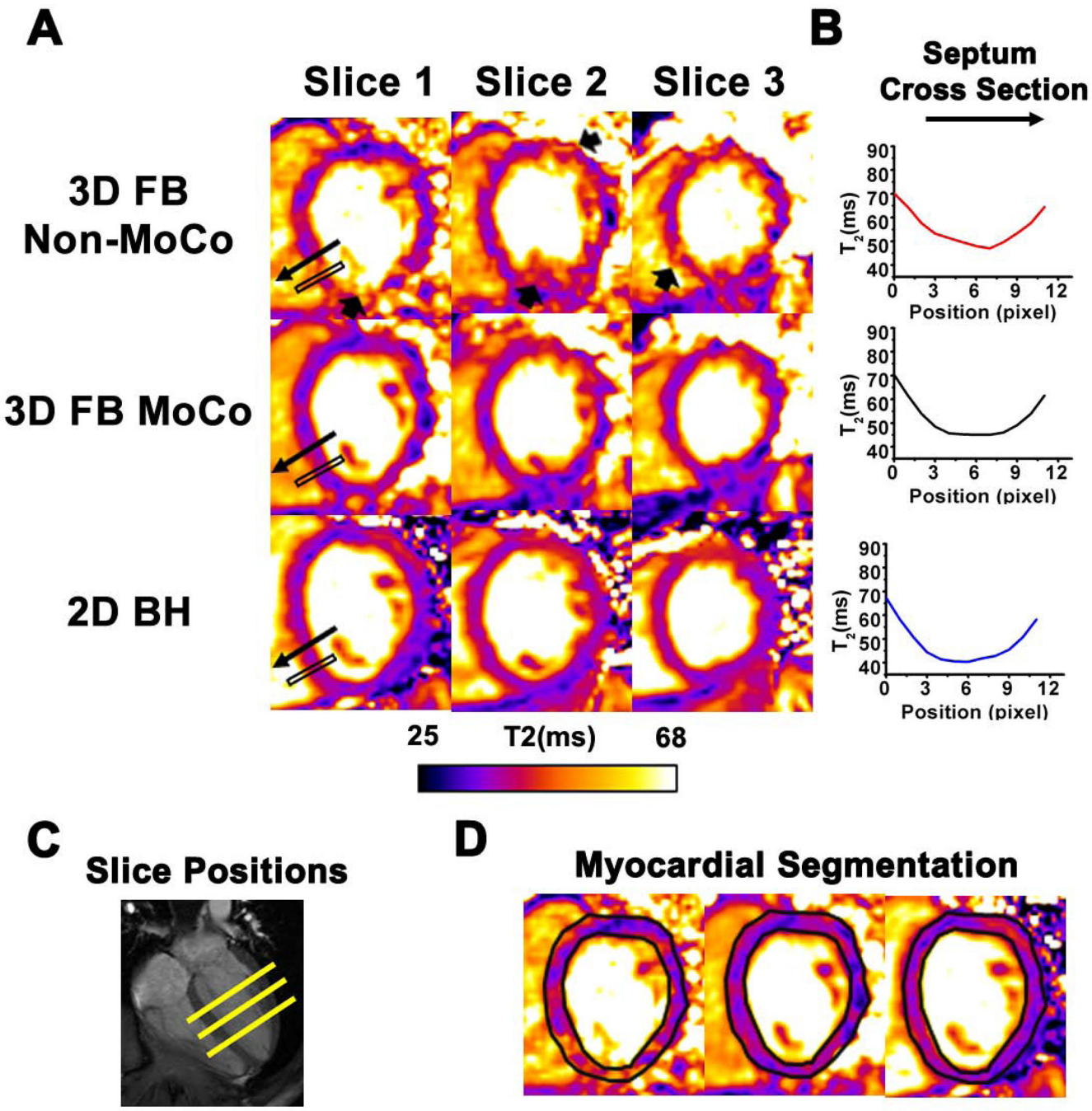

Fig. 4. Representative short-axis T_2 maps and T_2 profile across a representative region in the septum acquired from a healthy volunteer using 2D BH, 3D FB MoCo and 3D FB Non-MoCo approaches

T_2 maps reconstructed using weighted images from the different TEs at the three short-axis positions are shown in panel A. Note the loss of detail and variation in signal intensity in 3D FB Non-MoCo images (arrows), which is absent in 3D FB MoCo and 2D BH T_2 maps. In panel B, T_2 profile within the black box containing the septal wall of slice 1 is shown. In the 3D FB Non-MoCo profile, T_2 was significantly higher and showed larger deviation in the myocardial region relative to 3D FB MoCo and 2D BH. Corresponding slice positions of the

short-axis images along the long axis of the heart (C) and representative myocardial segmentation contours (D) are also shown for reference.

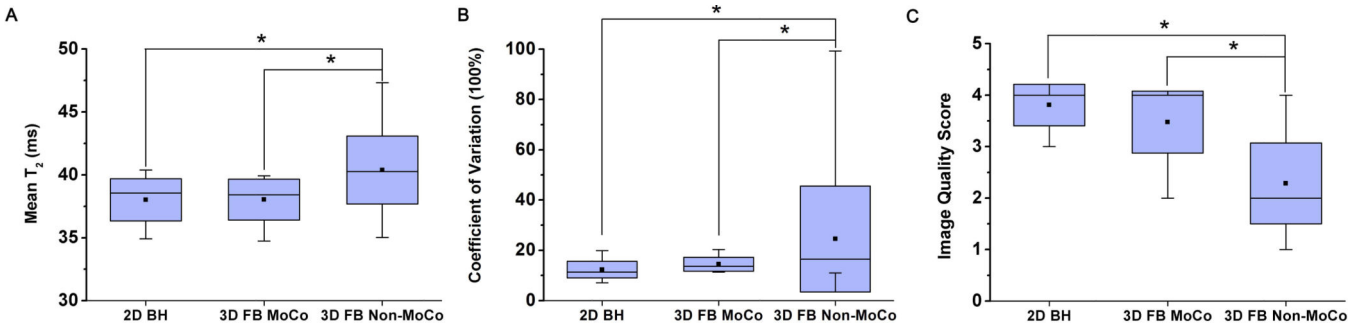

Fig. 5. Quantitative measures of mean T_2 (A), COV T_2 (B) and Image Quality scores (C) between 2D BH, 3D FB MoCo and 3D FB Non-MoCo approaches obtained from healthy volunteers

Across all measures, 2D BH and 3D FB MoCo approaches were not different but both were significantly different (* represents $p<0.05$) from 3D FB Non-MoCo approach.

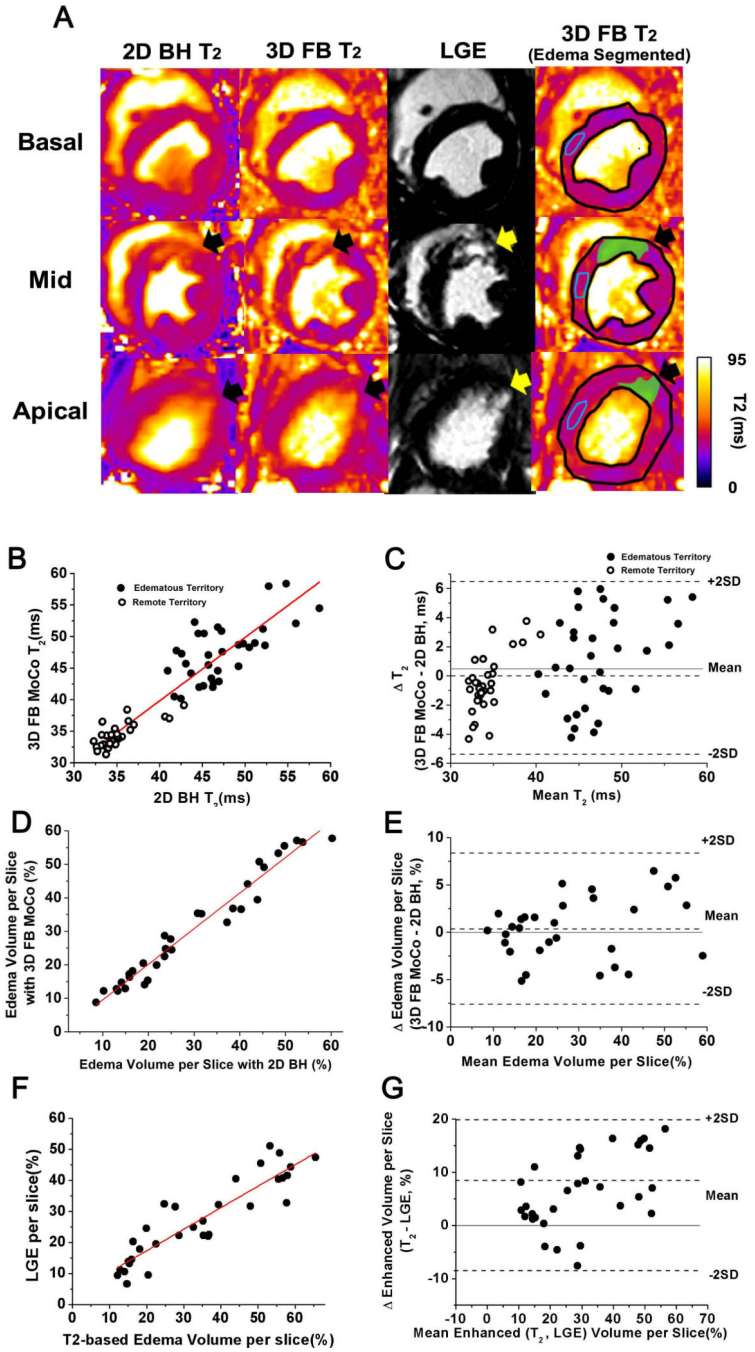

Fig. 6.

Representative short-axis images obtained from a canine on day 4 post-MI (A), the statistical relations between 2D BH and 3D MoCo for T_2 and edema volume and the statistical relations between T_2-based edematous and LGE volume across all animals (B–G). (A) Slice-matched T_2 maps from 2D BH and 3D FB MoCo, as well as LGE images obtained from a canine at the basal, mid ventricle (Mid) and apical sections are shown. Contours delineating the edematous volumes are presented in the right column. Note the close correspondence between hyperintense regions identified on 2D BH and 3D FB MoCo T_2

maps (black arrows) and their relation to hyperintense regions in LGE images (yellow arrows). Also note that the 2D BH images are blurrier due to cardiac motion (due to single-shot acquisitions in the presence of high heart rates in canines with recent infarction), which is not the case with the proposed approach. Linear regression analysis between T_2 values (edematous territories and remote myocardium) of slice-matched 3D FB MoCo and 2D BH acquisitions and the corresponding Bland-Altman analysis are shown in panels B and C, respectively. Linear regression: $y = 0.9\ x - 3.4$, where $y = T_2$ from 3D FB MoCo and $x = T_2$ from 2D BH acquisitions, with $R^2 = 0.88$, $p<0.05$ and bias = 0.8 ms. Linear regression analysis between slice-matched 3D FB MoCo and 2D BH acquisitions for Edema volume and the corresponding Bland-Altman analysis are shown in panels D and E, respectively. Linear regression: $y_1 = 1.1\ x_1 - 2.4$, where y_1 = Edema volume from 3D FB MoCo and x_1 = Edema volume from 2D BH acquisitions, with $R^2 = 0.96$, $p<0.05$ and bias = 0.6%. Linear regression analysis between slice-matched 3D FB MoCo Edema and LGE volume and the corresponding Bland-Altman analysis are shown in panels F and G, respectively. Linear regression: $y_2 = 0.7\ x_2 - 3.4$, where y_1 = LGE volume and x_1 = Edema volume from 3D FB MoCo acquisitions, with $R^2 = 0.8$, $p<0.05$ and bias = 8%.

Table 1

Performance of 2D-BH, 3D-FB-MoCo and 3D-FB-Non-MoCo in humans

Sequence / Subject	2D-BH	3D-FB-MoCo	3D-FB-Non-MoCo
T_2	38.0±1.7 ms	37.7±2.0 ms	40.3±2.7 ms*
COV	15±4 %	17.3±3 %	38±55 %*
IQ	3.8±0.4	3.5±0.6	2.3±0.8*

(* denote $p<0.05$)